Angular dynamics of the asteroid Geograhpos

Vladislav Borodin[1], Mikhail Bubenchikov[2], Alexey Bubenchikov[2], Dmitriy Mamontov[2], Soninbayar Zhambaa[3]
[1] Gazprom transgaz Tomsk LLC, Russia
[2] National Research Tomsk State University, Russia
[3] National University of Mongolia, Ulanbaatar, Mongolia
orevaore@mail.ru
(Submitted on 9.04.2025; Accepted on 3.07.2025)

Abstract. The paper shows that the inclined rotations of all triaxial elongated bodies lead to their π-tumbling around the axis with a minimum moment of inertia. The object (1620) Geographos, being the most elongated body in the Solar System, demonstrates a unique set of spin states due to its unusual shape; using the hodograph of the instantaneous angular velocity vector on the Poinsot plane, an interpretation of the complex spherical motions of the object under consideration is given. Based on this, two modes of complex rotations of the asteroid are identified.
Key words: Asteroid, Mathematical Modeling, Geographos, Classical Mechanics, Rotation.

Introduction

Object (1620) Geographos is a small near-Earth asteroid from the Apollo group, belonging to the spectral class S. It was discovered on September 14, 1951 by American scientists Rudolf Minkowski and Albert Wilson at the Palomar Observatory. In 1994, at the moment of the closest approach to Earth in the last two centuries (closer than 5 million km), radar studies of this body were carried out, during which a series of images were obtained. It turned out that the asteroid has the most elongated shape among all known bodies in the Solar System. Radar studies have shown that the light curve of this asteroid has deep minima and changing periodicity [1,2], which indicates the complex nature of its rotation. In paper [3], polarimetric and photometric observations of the object (1620) Geographos were carried out over four nights in September 1994. The observation results are compared with the spectral dependence of the inversion angle for (4179) Toutatis. After applying synchronous photometry, a composite light curve of the object 1620 Geographos was obtained. In paper [4], new photometric observations of the asteroid (1620) Geographos were carried out in 2000. It is shown that models with a constant period cannot satisfactorily describe the entire set of data on the light curves. Of great interest was the angular dynamics of the interstellar space object (1I/2017) Oumuamua. The data obtained in [5] demonstrate the widest range of variations in the object's brightness, which suggests an elongated shape of the body and the presence of complex revolutions in its motion. In paper [6], preference is given to the disk model for Oumuamua. In this paper, the tumbles are explained by the presence of torque due to gas release. In papers [7,8], binary asteroid systems are studied. Particular attention is paid to resonance in such systems. The study [9] presents the results of applying the Monte Carlo method to determine the absolute magnitudes and tilt parameters for 240,000 asteroids observed by the Pan-STARRS1 telescope during the first 15 months of its three-year all-sky survey mission. Goldstone radar observations of Geographos from August 28 to September 2, 1994, presented in [10], allowed us to

determine that the shape of the studied asteroid is extremely elongated. Estimates of the surface volumetric density of the object are presented. In [11], an improved thermophysical model was used to specify the thermophysical properties of Geographos. The obtained data are used to make detailed predictions of the Yarkovsky orbital drift and rotational acceleration (YORP effect), which are then compared with published measurements to determine the volumetric density of Geographos. In [12], using archival light curves and new photometric observations for the asteroids (10115) 1992 SK, (1620) Geographos and (1685) Toro, the class of asteroids was expanded with respect to the YORP effect. The values of the constant secular rotation accelerations were found for all three asteroids considered. In [13], Harris proposed a new thermal model for estimating the albedo and diameters of near-Earth asteroids (including Geographos). In [14], a physical model of the asteroid 1620 Geographos was developed using Goldstone and Doppler delayed radar images obtained in August 1994. In [15], the light curves of 16 asteroids, including 1620 Geographos, were analyzed. The photometric data were obtained at the Hunters Hill Observatory and at stations collaborating with it. The results of the processing were used to determine the synodic period and the amplitude of brightness variations. The authors [16] presented the results of a photometric study of 46 asteroids, one of which was Geographos. The study was conducted at the Lowell Laboratory for the period from 01.05.2008 to 31.12.2008. Warner [17] processed the light curves of 36 near-Earth asteroids. The data were obtained at the Solar System Research Center station from October to December 2015. Dunlap [18] processed the 1969 data for the asteroid 1620 Geographos. He noted that there is an unexplained change in the time of the appearance of minima. He concluded that the rotation is retrograde and determined the tilt of the rotation axis. Paper [19] presents the results of BVRIZ photometry of 56 near-Earth objects obtained using the 1-meter Jacobus Kapteyn telescope on La Palma Island in 2000 and 2001. Paper [20] reports that the YORP effect can spin up or twist asteroids with a radius of 5 km on a time scale of 10^8 years. This effect explains the rapid rotation of 1566 Icarus and the slow motion of 4179 Toutatis. The YORP effect is also quite applicable to explain the slow rotation of 253 Mathilde. In paper [21] the authors report a change in the rotational velocity of asteroid 1862 Apollo that is best explained by the YORP mechanism. The change is clearly visible in the photometric light curves. It amounts to one additional cycle in only 40 years. Paper [22] introduces the values of angular velocity with time according to a linear law. A total of 94 light curves observed in 1969-2008 were used to optimize the two parameters in this law. An excellent agreement between the observations and the model was obtained. This confirms the correct trend of the long-term influence of weak thermal torques. However, at present, the rotations of Geographos are not simple and are therefore characterized by several frequencies. In [23], it is demonstrated that the continuous increase in the rotational velocity of the near-Earth asteroid (43409) 2000 PH5 can well be attributed to the sunlight-induced torque (YORP effect). The detected spinning confirms the anomalous nature of the rotation velocity distribution of asteroids with diameters of 10 kilometers. The YORP effect demonstrates secular variations in the rotation velocity. This effect is capable of changing the position of the rotation axis and, as a consequence, leading to a change in the regime of complex rotations. However, there is a whole set of fundamental spin states determined only by

the shape of the object. These are the spin states that an elongated body of a given shape will have if it is spun at a certain angle between its long axis and the initial axis of rotation. We find these states in this paper. In [24-26], the coordinate approach to determining the orientation of a body in space presented in this study is used to analyze the rotations of carbon framework structures and crystalline grains of iron.

The purpose of this paper is to determine the complete set of fundamental spin states of the inertial motion of the asteroid (1620) Geographos.

1. Mesh model of the body

If three diameters of a body are known $d_1 = 5$ km; $d_2 = 2.1$ km; $d_3 = 2$ km, then the geometrical shape can be approximately reconstructed from a flat image and these three diameters. To do this, one must select the large diameter of the object and take the coordinates of two half-contours. Let ξ be the coordinate measured along the large diameter of the flat image, and $\{\xi_i\}$ be a system of points lying on the large diameter; $\{\eta_1(\xi^i)\}$ and $\{\eta_3(\xi^i)\}$ are the coordinates taken from the upper and lower half-contours. Let $\{\eta_2(\xi^i)\}$ and $\{\eta_4(\xi^i)\}$ be the coordinates of the upper and lower half-contours of the angle perpendicular to the original. If we do not have an image corresponding to the second angle, then we proceed as follows: $\{\eta_2(\xi^i)\} = k\{\eta_1(\xi^i)\}$; $\{\eta_4(\xi^i)\} = k\{\eta_3(\xi^i)\}$, where $k = \frac{d_3}{d_2}$. The first parameter of the grid surface was the coordinate ξ. The second parameter will be the angle φ (the angle between the planes passing through the ξ axis). Piecewise linear interpolation between the distributions of the four semi-contours is performed using the angle φ, which in a form that does not contain superscripts looks like this:

$$\begin{aligned}
\eta &= \eta_1 + \frac{2\varphi}{\pi}(\eta_2 - \eta_1), \quad 0 \le \varphi < \frac{\pi}{2} \\
\eta &= \eta_2 + \frac{2(\varphi - \frac{\pi}{2})}{\pi}(\eta_3 - \eta_2), \quad \frac{\pi}{2} \le \varphi < \pi \\
\eta &= \eta_3 + \frac{2(\varphi - \pi)}{\pi}(\eta_4 - \eta_3), \quad \pi \le \varphi < \frac{3\pi}{2} \\
\eta &= \eta_4 + \frac{2(\varphi - \frac{3\pi}{2})}{\pi}(\eta_1 - \eta_4), \quad \frac{3\pi}{2} \le \varphi < 2\pi
\end{aligned} \tag{1}$$

Absolute coordinates of points on the body surface are calculated using the following formulas:

$$\begin{aligned}
x^{i,j} &= x_i^i, \\
y^{i,j} &= \eta^{i,j} \sin\varphi^i, \\
z^{i,j} &= \eta^{i,j} \cos\varphi^i
\end{aligned} \tag{2}$$

The mesh surface obtained in this way is shown in Fig. 1 (right).

2. Equations of angular motion

At each moment in time, the velocity of the points of the grid frame representing the shape is completely determined by the velocity of the object $\boldsymbol{\omega} = (\omega_x, \omega_y, \omega_z)$:

$$\frac{d\boldsymbol{r}}{dt} = \boldsymbol{\omega} \times \boldsymbol{r}_i (i = \overline{1, N}). \tag{3}$$

Here $\boldsymbol{r}_i$=(x_i, y_i, z_i) is the radius vector of a separate point of the body, measured from its center of mass; N is the number of points constituting the body. Equations (3) are integrated under the following initial conditions:

$$t = 0, \boldsymbol{r}_i = \boldsymbol{r}_i{}^0 (i = \overline{1, N}). \tag{4}$$

During inertial rotation, the vector of the kinetic moment K retains its magnitude and direction in space. Therefore, we can write:

$$\boldsymbol{K}=\boldsymbol{J}\boldsymbol{\omega}=\boldsymbol{J}^0\boldsymbol{\omega}^0 = const. \tag{5}$$

Here $\boldsymbol{J} = \begin{pmatrix} A & F & E \\ F & B & D \\ E & D & C \end{pmatrix}$, is the tensor of inertia of a rotating body,

$$\begin{aligned} A = \sum (y_i^2 + z_i^2), B = \sum (x_i^2 + z_i^2), C = \sum (x_i^2 + y_i^2) \\ D = -\sum m_i y_i z_i, E = -\sum m_i x_i z_i, F = -\sum m_i x_i y_i. \end{aligned} \tag{6}$$

Vector equation (5) is used to determine ω. This equation is equivalent to a system of three scalar algebraic equations with the right-hand side determined by conditions (4), as well as the initial condition:

$$t=0, \boldsymbol{\omega} = \boldsymbol{\omega}^0. \tag{7}$$

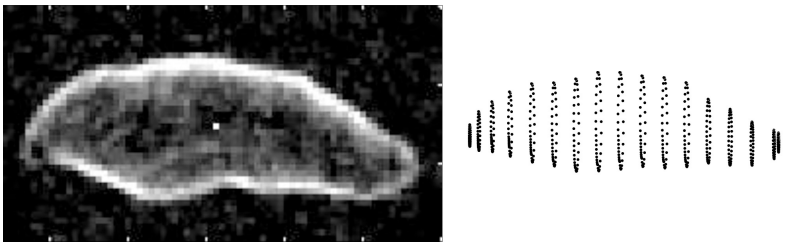

Fig. 1. Image of the asteroid Geographos (left) and its grid model (right)

The method presented in this section has been used in previous molecular dynamics studies [24-26] and has proven itself to be successful.

3. Non-dimensionalization and scheme of numerical solution of the problem

It is easy to see that the formulation of the problem of inertial rotation (3)-(7) is invariant with respect to the following transformations of variables:

$$\begin{aligned} t' = \omega^0 t, \quad \boldsymbol{\omega}' = \frac{\boldsymbol{\omega}}{\omega^0}, \\ \boldsymbol{r_{i'}} = \frac{\boldsymbol{r_i}}{R}, \quad m_{i'} = \frac{m_i}{m}. \end{aligned} \tag{8}$$

Here ω^0 is the value of the initial angular velocity of rotation of the body, R is the radial scale of the body, m^* is the characteristic mass of the particles that make up the body. From this invariance follows immediately the independence of inertial rotations from the absolute dimensions and total mass of the body and even with the corresponding compression (expansion) of time from the value of the initial rotational velocity. Inertial forces, caused by the tensor nature of the mass distribution in space, do not have a gravitational nature; therefore, in systems with different gravity, they will be the same. Due to the universality of the manifestation of these forces, inertial rotations, perceived as a system of spin states, will be called fundamental rotations of a body of complex shape.

It turned out that for elongated bodies, the family of spin states is one-parameter, i.e., it depends only on the angle between the long axis of the body and the axis of the initial rotation. Hereinafter, this is the angle δ. Moreover, the complete set of spin states is determined by the interval $\delta \in [0, \pi/2]$. On the intervals adjacent to this one, the same rotational states are determined by the mirror-symmetrical arrangement of the angle δ with respect to the preceding interval. In other words, there is no need to consider the intervals $[\pi/2, \pi]$, $[\pi, 3\pi/2]$, $[3\pi/2, 2\pi]$. All calculations are performed in the absolute coordinate system with respect to the angular displacements and in dimensionless variables (8). The time interval on which the trajectories are constructed is equal to 100 dimensionless units, which corresponds to one hundred dimensional periods of $1/\omega^0$. This period is sufficient to consider all events of the nearest future (the period of rotation of the Geographos is $1/\omega^0 = 5.2$ hours).

4. Numerical integration scheme

The evolution equations (3) are integrated using the classical fourth-order Runge-Kutta scheme for accuracy. However, when applying it at each time step and even at each intermediate position within a single step, the algebraic equations (5) are solved. This solution can be written in the form: $\boldsymbol{\omega} = \boldsymbol{J}^{-1}(\boldsymbol{J}^0\boldsymbol{\omega}^0)$. Here, $\boldsymbol{J}^{-1}$ denotes the inverse inertia tensor matrix. The synthetic combination of two standard algorithms produces a synergistic effect on the accuracy of solving the complete problem. The small integration step of $\Delta t' = 10^{-6}$ also significantly contributes to maintaining a low error in solving the defined equations. On the entire calculation interval, the relative errors in calculating the projections of the kinetic moment and the rotational energy do not exceed

$5 \cdot 10^{-15}$ dimensionless units (Fig. 2). This is practically machine accuracy of calculations, equal to the numerical interpretation of exact solutions. The calculations reproduced all spin states of the grid shape of the asteroid 1620 Geographos.

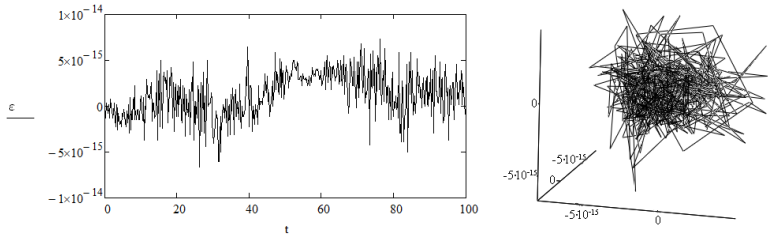

Fig. 2. Error in calculating the relative values of the kinetic energy of rotations (left) and the relative values of the projections of the kinetic values of the projections of the kinetic moment: (right).

In fig. 2 on the left, the error is calculated as $\varepsilon = \frac{T-T^0}{T^0}$, and on the right as $K'_x = \frac{K_x - K_x^0}{K^0}$, $K'_y = \frac{K_y - K_y^0}{K^0}$, $K'_z = \frac{K_z - K_z^0}{K^0}$. Here K_x, K_y, and K_z are the projections of the kinetic moment on the axes of the absolute basis, and K^0 is the constant value of the modulus of the kinetic moment. The superscript "0" marks the initial values of the calculated quantities.

5. Results of calculations of inclined rotations of the object

Conducted high-precision calculations have shown that for any inclinations of the major diameter to the initial axis of rotation, any body with a homogeneous density with a shape close to the considered asteroid experiences flips with respect to the long axis, i.e., it has repeatable, reproducible complex rotations. The methodology for finding a set of spin states of an object consists of a simple enumeration of its initial positions. We determine these positions by preliminary rotations of the body by an angle of α (around the X axis) and γ (around the Z axis). In this case, the basic position of the body is the position when the trihedron of the main axes of the body coincides with the trihedron of the absolute basis. Preliminary rotations of the body fix the initial positions of the coordinates of its centers of mass. We begin calculating each of the specific examples of motion at $\boldsymbol{\omega}^0 = (0, 1, 0)$. This means that the initial rotation is always performed around the Y axis. Therefore, preliminary rotations of the body around the Y axis (β-rotations) will not matter. If the vector of dimensionless angular velocity remains the same at subsequent moments of time, then a simple rotation of the object is realized. If noticeable values of the first and third components of the angular velocity are generated, then the spherical motion is complex. It is convenient to consider a complex spherical motion on the Poinsot plane, perpendicular to the constant vector

of the angular momentum K. The curves that the end of the vector ω draws on this plane are herpolhode. They are shown in Fig. 4. Thus, the entire space of the initial positions of the body will be two-parameter (two defining angles α and γ). Calculations have established that in the case of elongated bodies, γ-preliminary rotations generate dominant spin states. This means that in the case of successive non-commutative $\alpha\gamma$-preliminary rotations, everything will be determined by the resulting angle γ. Consequently, α-preliminary rotations can be excluded from consideration. Fig. 3 shows the trajectories of one of the points of the grid body, which has the maximum distance from its center of mass. These trajectories were obtained for different inclinations of the major axis of the object to the axis of initial rotation. The curves are located from left to right and top to bottom in decreasing order of the angle δ ($\delta = \pi/2 - \gamma$). The first trajectory (upper left angle $\delta = 90°$) corresponds to the case of rotation around the intermediate axis of inertia. In this example, over a time interval of one hundred periods $1/\omega^0$, there are 3 π-reversals around the axis with the minimum moment of inertia. In the case of $\delta = 75°$, ten π-reversals are observed. At $\delta = 60°$, the number of π-reversals becomes equal to 16. When $\delta = 45°$, there are 20 π-reversals. At $\delta = 30°$, 24 π-reversals are recorded. In the case of $\delta = 15°$, there are already 27 such revolutions in the interval of 100 dimensionless time units. Then the number of revolutions does not change, and at $\delta = 1°$, this number reaches the maximum value of 28 π-revolutions.

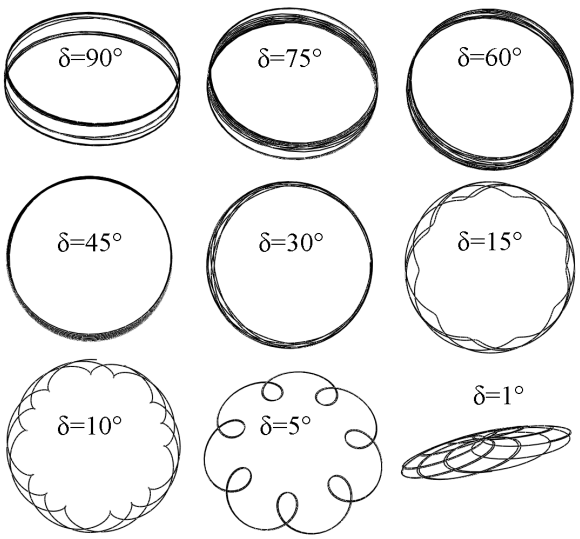

Fig. 3. Trajectories of a single point of the grid model at different angles of inclination of the long axis to the axis of the initial rotation.

It was mentioned above that during inertial rotation the vector of kinetic moment remains constant during the entire time of motion. This means that there is an unchangeable plane perpendicular to this vector. On this plane

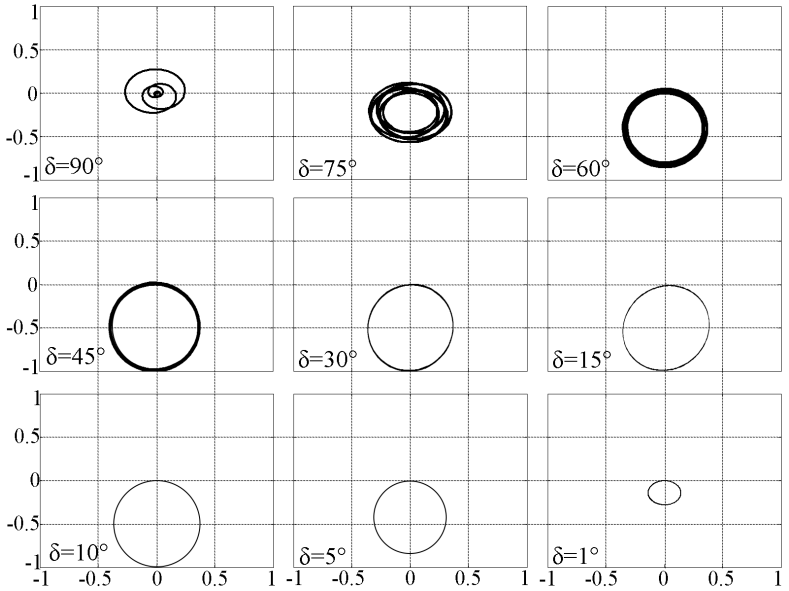

Fig. 4. Herpolhodes of complex rotations for δ from 90° to 0°.

the end of the instantaneous angular velocity vector will describe curved lines (herpoles) representing complex rotations of a rigid body. This idea was used by Louis Poinsot in his geometric interpretation of spherical motions. In Fig. 4, in the same order by decreasing angle δ, the herpoles of Geographos rotations are presented. At angles $\delta \in [60°, 90°]$, a wide precession ring is fixed, in which double logarithmic spirals are concentrated, forming complete rotation cycles. Each complete cycle corresponds to one π-revolution.With a decreasing value of δ located in the interval $\delta \in [30°, 45°]$, the herpole ring degenerates into a precession contour. At the same time, the size of the contour begins to increase. At $\delta \in [15°, 30°]$, the circle has a constant radius. At δ decreasing in the interval $\delta \in [0°, 15°]$, the size of the precession ring also decreases. Moreover, they decrease not to zero, but to the values shown in the last fragment of Fig. 4 (bottom right).

Since the points located on the axis of rotation of the body have no velocity, the herpolhode, which is the trajectory of the motion of the end of the instantaneous angular velocity vector, will simultaneously be a fixed centroid. At $\delta = 0°$ (this is the case of rotation around the long axis), the circular precession of the small ring remains. This remarkable case is shown separately in Fig. 5. It is interesting that when rotating around the axis with a minimum moment of inertia, the body makes somersaulting movements around the same axis. These somersaults have a fairly large amplitude (Fig. 5, left). As a result, the average velocity of the initial rotation decreases (Fig. 5, right). Here, the straight line shows the average value of the velocity, which shows that for a body of the shape under consideration, the rotation slows down by 6.5%. Since for elongated bodies the rotation system is reduced to a set of states corre-

sponding to a change in the angle δ from the interval $[0, \pi/2]$, it is easy to estimate the probability of implementing a specific mode by the length of the angular range that determines the selected mode. The simplest classification of modes can be obtained from Fig. 4.

First, there is a mode of a wide circular precession ring determined by the range $\delta \in [\pi/3, \pi/2]$, which is 33% of the basic interval of length $\pi/2$. This means $P_1 = 1/3$. In all other cases, we obtain a mode of contour precession. Therefore, the probability of realizing the second state of rotation is: $P_2 = 2/3$.

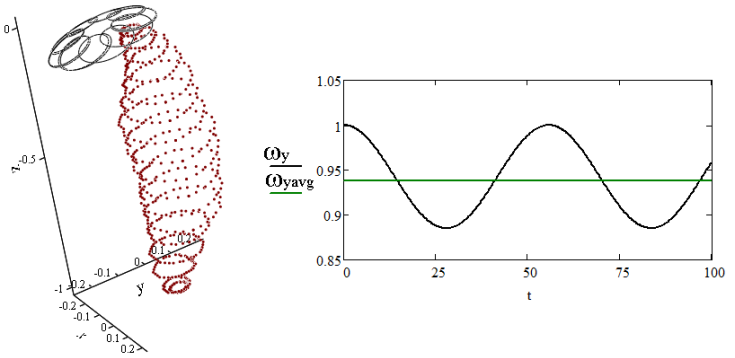

Fig. 5. The case of rotation around an axis with a minimum moment of inertia.

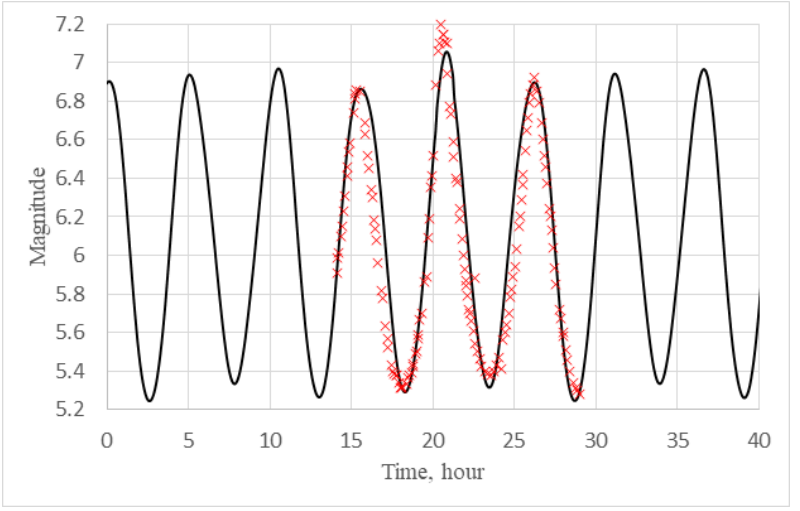

Fig. 6. Calculated light curve and observational data.

The observational data were taken from the catalogue[27]. The calculated light curve was constructed at $\delta = 29°$. In this case, the values of the minima and maxima of the light curve were the most consistent. Moreover, the calculated light curve was modelled with the assumption that the albedo of the body is the same for the entire surface of the asteroid. This fact explains the not quite exact correspondence between the calculated and observational curves. If necessary, the albedo distribution can also be taken into account.As the angle decreases further, the spread of amplitudes on the light curve will increase.

Conclusion

For a body of such a peculiar shape as the object (1620) Geographos, no rotations are simple. Different directions of the long axis of the body relative to the axis of the initial rotation generate a system of different spin states of the object. These motions are accompanied by precession of the instantaneous axis of rotation, or precession with significant nutation swings, ending with flips of the body around the axis with a minimum value of the moment of inertia. Thus, in the rotations of the asteroid Geographos, one can distinguish a regime of a wide precession ring and contour precession. Geographos, depending on the location of its long axis relative to the vector ω^0, experiences from three to twenty-eight π-flips over a time interval of $100/\omega^0$. These flips determine the second frequency of complex spherical motion, which can be used to explain changes in the light curve. Rotation around the long axis of the object in question is also not simple. In this case, the instantaneous axis of rotation wobbles, which leads to the effect of slowing down the axial rotation. For all elongated bodies, due to the presence of dominant and weak rotation states, the two-parameter system of spin states is reduced to a one-parameter one.

References

Prokofeva V. V., Karachkina L. G., Taraschuk V. P., 1997, *Investigations of oscillations in the brightness of Asteroid 1620 Geographos during its approach to the Earth in 1994*, Astronomy Letters, Vol. 23, No. 6, pp. 758767.

Karachkina L. G., Prokofeva V. V., Taraschuk V. P., 1998, *Modulations of brightness of Asteroid 1620 Geographos*, Solar System Research, Vol. 32, pp. 287298.

Vasiliev S. V., Lupishko D. V., Shahosvkiy N., Efimov Yu. S., 2000, *UVVRI polarimetry and photometry of asteroid 1620 Geographos*, Kinematics and Physics of Celestial Bodies, No. 4, pp. 1318.

urech J., Vokrouhlick D., Kaasalainen M., Higgins D., Krugly Yu. N., Gaftonyuk N. M., Shevchenko V. G., Chiorny V. G., Hamanowa H., Reddy V., Dyvig R. R., 2008, *Detection of the YORP effect in asteroid (1620) Geographos*, A&A, Vol. 489, Issue 2, pp. L25L28, DOI: https://doi.org/10.1051/0004-6361:200810672.

Bolin B., Weaver H., Fernandez Y., Lisse C., Huppenkothen D., Jones L., Juric M., Moeyens J., Schambeau C., Slater C., Ivezic Z., Connolly A., 2017, *APO Time Resolved Color Photometry of Highly-Elongated Interstellar Object 1I/'Oumuamua*, The Astrophysical Journal, Vol. 852, DOI: 10.3847/2041-8213/aaa0c9.

Mashchenko S., 2019, *Modelling the light curve of Oumuamua: evidence for torque and disc-like shape*, Monthly Notices of the Royal Astronomical Society, Vol. 489, Issue 3, pp. 30033021, DOI: https://doi.org/10.1093/mnras/stz2380.

Lei H., 2024, *Spinorbit coupling of the primary body in a binary asteroid system*, Celestial Mechanics and Dynamical Astronomy, Vol. 136, 37, DOI: https://doi.org/10.1007/s10569-024-10211-5.

Rosaev A., 2024, *Resonance perturbation of (5026) Martes and 2005 WW113 asteroid pair*, Celestial Mechanics and Dynamical Astronomy, Vol. 136, 41, DOI: https://doi.org/10.1007/s10569-024-10209-z.

Veres P., Jedicke R., Fitzsimmons A., Denneau L., Granvik M., Bolin B., Chastel S., Wainscoat R., Burgett W., Chambers K., Flewelling H., Kaiser N., Magnier E., Morgan J., Price P., Tonry J., Waters C., 2015, *Absolute magnitudes and slope parameters for 250,000 asteroids observed by Pan-STARRS PSI - Preliminary results*, Icarus, Vol. 261, DOI: 10.1016/j.icarus.2015.08.007.

Ostro S. J., Jurgens R. F., Rosema K. D., Hudson R. S., Giorgini J. D., Winkler R., Yeomans D. K., Choate D., Rose R., Slade M. A., Howard S. D., Scheeres D. J., Mitchell D. L., 1996, *Radar Observations of Asteroid 1620 Geographos*, Icarus, Vol. 121, No. 1, pp. 4666, DOI: 10.1006/icar.1996.0071.

Rozitis B., Green S., 2014, *Physical characterisation of near-Earth asteroid (1620) Geographos*, Astronomy and Astrophysics, Vol. 568, DOI: 10.1051/0004-6361/201323090.

Durech J., et al., 2021, *Rotation acceleration of asteroids (10115) 1992 SK, (1685) Toro, and (1620) Geographos due to the YORP effect*, Astronomy and Astrophysics, Vol. 657, DOI: 10.1051/0004-6361/202141844.

Harris A. W., 1998, *A Thermal Model for Near-Earth Asteroids*, Icarus, Vol. 131, No. 2, pp. 291301, DOI: 10.1006/icar.1997.5865.

Hudson R. S., Ostro S. J., 1999, *Physical Model of Asteroid 1620 Geographos from Radar and Optical Data*, Icarus, Vol. 140, No. 2, pp. 369378, DOI: 10.1006/icar.1999.6142.

Higgins D., 2008, *Asteroid Lightcurve Analysis at Hunters Hill Observatory and Collaborating Stations: November 2007 - March 2008*, Minor Planet Bulletin, Vol. 35, No. 3, pp. 123126.

Skiff B. A., Bowell E., Koehn B. W., Sanborn J. J., McLelland K. P., Warner B. D., 2012, *Lowell Observatory Near-Earth Asteroid Photometric Survey (NEAPS) - 2008 May through 2008 December*, Minor Planet Bulletin, Vol. 39, No. 3, pp. 111130.

Warner B. D., 2016, *Near-Earth Asteroid Lightcurve Analysis at CS3-Palmer Divide Station: 2015 October-December*, Minor Planet Bulletin, Vol. 43, No. 2, pp. 143154.

Dunlap J. L., 1974, *Minor planets and related objects. XV. Asteroid (1620) Geographos*, The Astronomical Journal, Vol. 79, p. 324, DOI: 10.1086/111546.

Dandy C. L., Fitzsimmons A., Collander-Brown S. J., 2003, *Optical colors of 56 near-Earth objects: Trends with size and orbit*, Icarus, Vol. 163, pp. 363373, DOI: 10.1016/S0019-1035(03)00087-3.

Rubincam D. P., 2000, *Radiative Spin-up and Spin-down of Small Asteroids*, Icarus, Vol. 148, No. 1, pp. 211, DOI: 10.1006/icar.2000.6485.

Kaasalainen M., urech J., Warner B., et al., 2007, *Acceleration of the rotation of asteroid 1862 Apollo by radiation torques*, Nature, Vol. 446, pp. 420422, DOI: 10.1038/nature05614.

Durech J., Vokrouhlick D., Kaasalainen M., Higgins D., Krugly Y., Gaftonyuk N., Shevchenko V., Chiorny V., Hamanowa H., Reddy V., Dyvig R., 2008, *Detection of the YORP effect in asteroid (1620) Geographos*, Astronomy and Astrophysics, Vol. 489, pp. L25L28, DOI: 10.1051/0004-6361:200810672.

Taylor P. A., Margot J.-L., Vokrouhlick D., Scheeres D. J., Pravec P., Lowry S. C., Fitzsimmons A., Nolan M. C., Ostro S. J., Benner L. A. M., Giorgini J. D., Magri C., 2007, *Spin Rate of Asteroid (54509) 2000 PH5 Increasing Due to the YORP Effect*, Science, Vol. 316, No. 5822, pp. 274277, DOI: 10.1126/science.1139038.

Bubenchikov M., Mamontov D., Azheev S., Azheev A., 2023, *Rotation of supermolecules around an intermediate axis of inertia*, Vestnik Tomskogo gosudarstvennogo universiteta. Matematika i mekhanika, pp. 4958, DOI: 10.17223/19988621/80/5.

Borodin V. I., Bubenchikov M. A., Bubenchikov A. M., et al., 2024, *Angular dynamics of molecular bodies*, Meccanica, DOI: https://doi.org/10.1007/s11012-024-01902-2.

Borodin V., Bubenchikov M., Bubenchikov A., Mamontov D., Azheev S., Azheev A., 2023, *Study of the Unstable Rotational Dynamics of a Tor-Fullerene Molecular System*, Crystals, Vol. 13, No. 2, p. 181, DOI: 10.3390/cryst13020181.

Lagerkvist C.-I., Magnusson P., Eds., 2011, *Asteroid Photometric Catalog V1.1*, EAR-A-3-DDR-APC-LIGHTCURVE-V1.1, NASA Planetary Data System.